

One-Center Charge Transfer Transitions in Manganites

A. S. Moskvin

Ural State University, 620083 Ekaterinburg, Russia

Abstract

In frames of a rather conventional quantum-chemical approach, which combines the crystal field and the ligand field models we have addressed different charge transfer (CT) states and $O2p - Mn3d$ CT transitions in MnO_6^{9-} octahedra. The many-electron dipole transition matrix elements were calculated using the Racah algebra for the cubic point group. Simple "local" approximation allowed to calculate the relative intensity for all dipole-allowed $\pi - \pi$ and $\sigma - \sigma$ CT transitions. We present a self-consistent description of the CT bands in $LaMnO_3$ which allows to correct the current interpretation of the optical spectra. Our analysis shows the multi-band structure of the CT optical response with the weak low-energy edge at 1.7 eV, associated with forbidden $t_{1g}(\pi) - e_g$ transition and a series of the weak and strong dipole-allowed high-energy transitions starting from 2.5 and 4.5 eV, respectively, and extending up to nearly 11 eV. The most intensive features are associated with two strong composite bands near 4.6 \div 4.7 eV and 8 \div 9 eV, respectively, resulting from the superposition of the dipole-allowed $\sigma - \sigma$ and $\pi - \pi$ CT transitions. These predictions are in good agreement with experimental spectra. The experimental data point to a strong overscreening of the crystal-field parameter Dq in the CT states of MnO_6^{9-} centers.

PACS codes: 71.10.-w, 71.15.-m, 71.15.Fv, 78.20.Bh

Keywords: Manganites, electron structure, charge transfer, optical spectra

1 Introduction

The discovery of the colossal magnetoresistance in doped manganites like $La_{1-x}Sr_xMnO_3$ have generated a flurry of ideas, models and scenarios of this puzzling phenomena, many of which are being developed up to date, although the situation remains controversial. There are many thermodynamic and local microscopic quantities that cannot be explained by the conventional double-exchange model with dominantly $Mn3d$ location of doped holes. In such a situation we argue a necessity to discuss all possible candidate states with different valent structure of manganese and oxygen atoms, as well as different valent states of octahedral MnO_6 centers [1]. Namely this slightly distorted octahedra is believed to be the basic unit both for crystalline and electronic structure.

As for an examination of the energy spectrum and electronic structure one should emphasize an importance of different optical methods because these provide valuable information concerning the dielectric function. The nature of the low-energy electron-hole excitations in the insulating transition metal (3d-) oxides represents one of the most important challenging issues for these strongly correlated systems. It is now believed that the most intensive low-energy electronic excitations in insulating 3d-oxides correspond to the transfer of electrons from oxygen anion to 3d metal cation, hence these materials are charge transfer (CT) insulators. However, the more detailed assignment of these excitations remains open. All these are especially interesting because they could play a central role in multiband Hubbard models used to describe both the insulating state and the unconventional states developed under electron or hole doping.

It is now generally accepted that the ground state of the MnO_6 centers in $LaMnO_3$ corresponds to the orbital doublet 5E_g term of the high-spin $t_{2g}^3e_g^1$ configuration. The optical conductivity spectrum of $LaMnO_3$ exhibits two broad peaks centered around 2.0 and 5.0 eV [2, 3, 4, 5]. However, it has remained unclear just what the nature of the intensive low-energy optical electron-hole excitation peaked near 2.0 eV as well as more intensive excitations with higher energy peaked near 5.0 eV. Some authors [2, 3, 5] assign these both features to the dipole-allowed CT transitions like $t_{2g}^3e_g^1 - t_{2g}^3e_g^2\underline{L}$ and $t_{2g}^3e_g^1 - t_{2g}^4e_g^1\underline{L}$ (\underline{L} denoting a ligand hole), respectively. However, others [4] assign the low-energy peak to the "intra-atomic" $^5E_g - ^5E_g'$ transition, or doubly-forbidden (parity and orbital quasimomentum) $d - d$ -like crystal-field transition between two 5E_g -sublevels separated by a splitting due to low-symmetry crystalline field. Such a rather big magnitude of the splitting is likely to agree with the observed magnitudes of the low-symmetry distortions for the MnO_6^{9-} octahedra in $LaMnO_3$. Both interpretations being particularly qualitative suffer from many shortcomings and give rise to many questions concerning the details of the charge transfer states, or expected extremely weak intensity for the $d - d$ transitions.

Unfortunately, the main body of the optical data for manganites is obtained from reflectivity measurements, that often implies a parasitic contribution due to a deterioration of the sample surface [3], and can give rise to some

ambiguities due to problems with Kramers-Krönig transformation. The more straightforward optical transmission spectra of the $LaMnO_3$ films [6] revealed a fine structure of the low-energy 2 eV band with two features near 1.7 and 2.4 eV, respectively, which were assigned in contrast with the preceding interpretations [2, 3, 4, 5] to the Mn^{3+} $d - d$ crystal-field transition $^5E_g - ^3T_{1g}$, splitted by the JT effect. Such an ambiguity leaves the question of the nature of the main optical transitions in $LaMnO_3$ far from being resolved. The band structure calculations, including the LDA+U, fail to clear up the situation because of these cannot reproduce the important effects of intra-atomic correlations forming the term structure both of ground and excited CT states.

In this connection a rather conventional quantum-chemical approach, which combines the crystal field and the ligand field models with real opportunity to include all correlation effects, seems more relevant.

Below, in frames of such an approach we address different CT states and $O2p - Mn3d$ CT transitions in MnO_6 octahedra. As we conjecture, namely these mainly define the optical response both for undoped $LaMnO_3$ and different doped manganites.

2 Electron structure of manganese ions and manganese-oxygen octahedral centers in manganites

5 manganese $Mn3d$ and 18 oxygen $O2p$ atomic orbitals in octahedral MnO_6 complex with the point symmetry group O_h form both hybrid $Mn3dO2p$ bonding and antibonding e_g and t_{2g} molecular orbitals (MO), and non-bonding $a_{1g}(\sigma)$, $t_{1g}(\pi)$, $t_{1u}(\sigma)$, $t_{1u}(\pi)$, $t_{2u}(\pi)$ ones [7, 8, 9, 10]. Non-bonding $t_{1u}(\sigma)$ and $t_{1u}(\pi)$ with the same symmetry are hybridized due to the oxygen-oxygen $O2p\pi - O2p\pi$ transfer. The relative energy position of different non-bonding oxygen orbitals is of primary importance for the spectroscopy of the oxygen-manganese charge transfer. This is firstly determined by the bare energy separation $\Delta\epsilon_{2p\pi\sigma} = \epsilon_{2p\pi} - \epsilon_{2p\sigma}$ between $O2p\pi$ and $O2p\sigma$ electrons. Since the $O2p\sigma$ orbital points towards the two neighbouring positive $3d$ ions, an electron in this orbital has its energy lowered by the Madelung potential as compared with the $O2p\pi$ orbitals, which are perpendicular to the respective $3d - O - 3d$ axes. Thus, Coulomb arguments favour the positive sign of the $\pi - \sigma$ separation $\epsilon_{p\pi} - \epsilon_{p\sigma}$ which numerical value can be easily found in the point charge model, and appears to be of the order of 1.0 eV. In a first approximation, all the $\gamma(\pi)$ states $t_{1g}(\pi)$, $t_{1u}(\pi)$, $t_{2u}(\pi)$ have the same energy. However, the $O2p\pi - O2p\pi$ transfer yields the energy correction to its bare energies with the largest in value and positive in sign for the $t_{1g}(\pi)$ state. The energy of $t_{1u}(\pi)$ state drops due to hybridization with cation $4pt_{1u}(\pi)$ state. In other words, the $t_{1g}(\pi)$ state is believed to be the highest in energy non-bonding oxygen state. For illustration, in Fig.1 we show the energy spectrum of the $3d - 2p$ manifold in octahedral complexes like MnO_6 with the relative energy position of the levels accordingly to the X_α -method calculations [11] for the FeO_6^{9-} octahedral complex in a lattice environment typical for perovskites like $LaFeO_3$, $LaMnO_3$.

Conventional electronic structure of octahedral MnO_6 complexes is associated with configuration of the completely filled $O2p$ shells and partly filled $Mn3d$ shells. The typical high-spin ground state configuration and crystalline term for Mn^{3+} in octahedral crystal field or for the octahedral MnO_6^{9-} center is $t_{2g}^3e_g^1$ and 5E_g , respectively. Namely this orbital doublet results in a vibronic coupling and Jahn-Teller (JT) effect for the MnO_6^{9-} centers, and cooperative JT ordering in $LaMnO_3$. In the framework of crystal field model the 5E_g term originates from the $(3d^45D)$ term of free Mn^{3+} ion. Among the low-energy crystal field $d - d$ transitions for the high-spin Mn^{3+} ions one should note a single spin-allowed and parity-forbidden $^5E_g - ^5T_{2g}$ transition at energy varying from about 2.0 to 2.5 eV depending on the crystalline matrix. So, this is likely to be near 2.5 eV for the Mn^{3+} impurity in perovskite $YAlO_3$ [12]. The transition is magneto-optically active, and could manifest itself in the Faraday and Kerr effects. A detection of the spin- and parity-forbidden $^5E_g - ^3T_{1g}$ transition with, probably, lower energy could be rather important in the Mn^{3+} assignment.

Unconventional electronic configuration of octahedral MnO_6 complexes is associated with a *charge transfer state* with one hole in $O2p$ shells. The excited CT configuration $\tilde{\gamma}_{2p}^1 3d^{n+1}$ arises from the transition of an electron from the MO predominantly anionic in nature (the hole $\tilde{\gamma}_{2p}$ in the core of the anionic MO being hereby produced), into an empty $3d$ -type MO (t_{2g} or e_g). The transition between the ground configuration and the excited one can be presented as the $\gamma_{2p} \rightarrow 3d(t_{2g}, e_g)$ CT transition.

The CT configuration consists of two partly filled subshells, the ligand γ_{2p} , and the cation $3d(t_{2g}^{n_1}e_g^{n_2})$ shell, respectively. It should be emphasized that the oxygen hole having occupied the *non-bonding* γ_{2p} orbital interact *ferromagnetically* with $3d(t_{2g}^{n_1}e_g^{n_2})$ shell. This rather strong (up to ~ 0.1 eV) ferromagnetic coupling results in Hund rule for the CT configurations, and provides the high-spin ground states. It should be noted that the maximal value of the total spin for the Hund-like CT state in MnO_6^{9-} center equals $S = 3$, that uncovers some perspectives to unconventional magnetic signatures of these states.

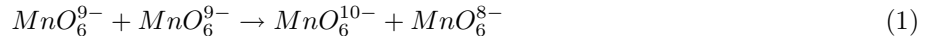
In addition, the quadrupole-quadrupole interaction between $3d^{n+1}$ shell and oxygen hole will result in the splitting of the levels with different values of the total orbital quasimomentum for the complex.

It should be noted that the presence of the oxygen hole moving around $3d$ -ion in the CT state can, in common, provides a strong screening both of the $3d$ crystalline field and intra-atomic electron-electron repulsion with the renormalization of the appropriate correlation Racah parameters A, B, C and crystal field splitting Dq . It should be noted that unlike the "monopole" parameter A the "multipole" ones B and C usually manifest relatively weak response to crystalline environment. Nevertheless, all these effects can strongly complicate the calculation of the energy structure for the respective $3d^{n+1}$ configuration. This configuration in the case of CT states in MnO_6^{9-} center nominally corresponds to Mn^{2+} ion. In Fig.2 we reproduce the conventional octahedral crystal field energy scheme (Tanabe-Sugano diagram) for the high-spin states of $3d^5$ configuration given the typical for Mn^{2+} ions in oxides parameters $B = 0.12$, $C = 0.41$ eV [14, 15]. It is well-known that the typical high-spin ground state configuration and crystalline term for Mn^{2+} in cubic crystal field or for the octahedral MnO_6^{10-} center is a half-filled configuration $t_{2g}^3 e_g^2$ and the orbital singlet term $^6A_{1g}$, respectively. In frames of crystal field model this term originates from the $(3d^5 \ ^6S)$ term of free Mn^{2+} ion. The strong Coulomb repulsion leading to the high-spin $^6A_{1g}$ ground term for Mn^{2+} ion would result in strong corrections to a simple picture of the energies for the CT states based on the one-electron approach sketched in Fig.1. Indeed, the one-electron model predicts the lower energy of the CT states with $3d^5; t_{2g}^4 e_g^1$ configuration rather than $3d^5; t_{2g}^3 e_g^2$ configuration. This example clearly demonstrates the role played by intra-atomic correlations. It should be noted that for the $3d^5$ configuration the $^6A_{1g}$ term is the only spin-sextet, so all the $d - d$ transitions from the ground state are spin- and parity-forbidden, therefore these are extremely weak (oscillator strength $\sim 10^{-7}$), and hardly observable in the optical absorption spectra. However, it has been recently shown (see Ref. [13] and references therein) that the dipole- and spin-forbidden $d - d$ excitations can be examined excellently by spin-polarized electron energy loss spectroscopy (EELS). Fromme *et al.* [13] have measured with high accuracy (≤ 0.02 eV) the excitation energies for almost all quartet $^4\Gamma$ terms of Mn^{2+} ions in MnO : $^4T_{1g}(^4G)$ (2.13), $^4T_{2g}(^4G)$ (2.4), $^4A_{1g}, ^4E_g(^4G)$ (2.82), $^4T_{2g}(^4D)$ (3.31), $^4E_g(^4D)$ (3.82), $^4T_{1g}(^4P)$ (4.57), $^4A_{2g}(^4F)$ (5.08), $^4T_{1g}(^4F)$ (5.38 eV). The energy of $^4T_{2g}(^4F)$ term is expected to be near 6.0 eV [14]. Simple textbook three-parameter (B, C, Dq) crystal field theory [16] provides self-consistent description of these data given the crystal field parameter $Dq = 0.15$ eV (see Fig.2). Rigorously speaking, we should conclude $Dq = \pm 0.15$ eV because the energies of all quartet and sextet terms for the half-filled $3d^5$ configuration depend only on modulus $|Dq|$. Parameter Dq defines not only the value of the cubic crystal field splitting $\Delta = 10Dq = E(e_g) - E(t_{2g})$, but its sign. In other words, measuring only the energy of quartet terms for Mn^{2+} (or Fe^{3+}) we cannot separate two opposite cases: $E(e_g) > E(t_{2g})$ and $E(e_g) < E(t_{2g})$. However, this puzzling effect concerns only the energy rather than wave functions for the 4T_g terms which are strongly depend on the sign of Dq . Given $Dq > 0$ the lowest $^4T_{1g}$ term is of dominant $t_{2g}^4 e_g^1$ configuration, while for $Dq > 0$ this is of dominant $t_{2g}^2 e_g^3$ configuration. Below we shall see that the latter effect would result in very strong difference in the lineshape of the CT bands for $Dq > 0$ and $Dq < 0$ given the same energy spectrum of the CT states.

Finally, one should emphasize that both the energy and wave functions for $^6A_{1g}, ^4A_{1g}, ^4A_{2g}, ^4E_g$ terms do not depend on crystal-field parameter Dq at all.

3 Charge transfer transitions for the MnO_6^{9-} centers.

A set of the intensive and broad absorption bands in parent manganites is related to the anion-cation $O2p - Mn3d$ charge transfer. In the framework of the MnO_6 center model this elementary CT process generates both intra- and inter-center CT transitions for the MnO_6^{9-} centers. The intra-center CT transitions could be associated with the *small CT Frenkel excitons* [17] and represent the oxygen hole moving around $3d^{n+1}$ -cation. The inter-center CT transitions form a set of *small CT excitons*, which in terms of chemical notions represent somewhat like the *disproportionation* quanta



resulting in a formation of the bounded electron MnO_6^{10-} (e -) and hole MnO_6^{8-} (h -) small radius centers. A minimal energy of such an exciton or the disproportionation threshold usually proves to be lower than appropriate purely ionic quantity which value equals to the electrostatic correlation energy $U_{dd} \approx 10$ eV.

3.1 Intracenter charge transfer transitions for the MnO_6^{9-} centers.

Conventional classification scheme of the CT transitions in the octahedral MnO_6^{9-} centers (intra-center CT transitions) incorporates the electro-dipole allowed transitions $\gamma_u \rightarrow 3dt_{2g}, 3de_g$ from the odd oxygen $\gamma_u = t_{1u}(\pi), t_{2u}(\pi), t_{1u}(\sigma)$ orbitals to the even manganese $3dt_{2g}$ and $3de_g$ orbitals, respectively. These one-electron

transitions generate a manifold of the many-electron ones ${}^5E_g \rightarrow {}^5T_u$ (T_u may be equal both to T_{1u} , and T_{2u}) which may additionally differ by crystalline term of the respective $3d^{n+1}$ configuration:

$$({t^3_{2g}}^4 A_{2g}; e_g^1) {}^5E_g \rightarrow (({t^4_{2g}}^3 T_{1g}; e_g^1) {}^4\Gamma_g; \underline{\gamma_u}) {}^5T_u, \quad (2)$$

$$({t^3_{2g}}^4 A_{2g}; e_g^1) {}^5E_g \rightarrow (({t^3_{2g}}^4 A_{2g}; e_g^2, {}^{2S_1+1}\Gamma_{1g}) {}^{2S+1}\Gamma_g; \underline{\gamma_u}) {}^5T_u \quad (3)$$

for $\gamma_u \rightarrow 3dt_{2g}$ and $\gamma_u \rightarrow 3de_g$ transitions, respectively. Here, we already took into account the Pauli principle and the "triangle rules" for spin momenta and orbital "quasi-momenta" like Γ . Proceeding with this analysis we can obtain full selection rules for the many-electron CT transitions:

1. Each $\gamma_u \rightarrow 3dt_{2g}$ transition generates two doublets of many-electron CT transitions ${}^5E_g \rightarrow {}^5T_{1,2u}$, differing by the term of the $t_{2g}^4 e_g^1$ configuration: ${}^4T_{1g}$ and ${}^4T_{2g}$, respectively.

2. Each $\gamma_u \rightarrow 3de_g$ transition generates 5 many-electron CT transitions ${}^5E_g \rightarrow {}^5T_{1,2u}$, differing by the term of the $t_{2g}^3 e_g^2$ configuration: ${}^4A_{1g}$, ${}^4A_{2g}$, ${}^6A_{1g}$, 4E_g , respectively (in the case of 4E_g term each one-electron transition generates the ${}^5T_{1,2u}$ doublet).

Additionally, we should take account for the configurational interaction. Indeed, the terms with the same symmetry for different configurations interact and mix with each other. In our case, for the $3d^5$ configuration we have 3 terms ${}^4T_{1g}$ and 3 terms ${}^4T_{2g}$ which present both in the $t_{2g}^4 e_g^1$ and $t_{2g}^3 e_g^2$, $t_{2g}^2 e_g^3$ configurations (see Fig.2). It should be noted, that for $t_{2g}^3 e_g^2$ configuration there are two interacting 4E_g terms.

Thus, beginning from $3t_{1u}(\pi), t_{1u}(\sigma), t_{2u}(\pi)$ non-bonding purely oxygen orbitals as initial states for one-electron CT we come to 60 many-electron dipole-allowed CT transitions ${}^5E_g \rightarrow {}^5T_{1,2u}$: 24 transitions $t_{1u}(\pi), t_{2u}(\pi) - t_{2g}$ ($\pi - \pi$ channel), 16 transitions $t_{1u}(\pi), t_{2u}(\pi) - e_g$ ($\pi - \sigma$ channel), 12 transitions $t_{1u}(\sigma) - t_{2g}$ ($\sigma - \pi$ channel), and 8 transitions $t_{1u}(\sigma) - e_g$ ($\sigma - \sigma$ channel), respectively.

3.2 Dipole transition matrix elements

Making use of the Racah algebra (the method of the irreducible tensorial operators) [18, 16, 19] both for spins and quasimomenta we may obtain after some cumbersome calculations for the transition matrix elements:

$\gamma_u \rightarrow t_{2g}$ transfer

$$\begin{aligned} & \langle ({t^3_{2g}}^4 A_{2g}; e_g^1) {}^5E_g \mu | \hat{d}_q | (({t^4_{2g}}^3 T_{1g}; e_g^1) {}^4\Gamma_g; \underline{\gamma_u}) {}^5T_u \mu' \rangle = \\ & (-1)^\mu \left\langle \begin{array}{ccc} E_g & T_{1u} & T_u \\ -\mu & q & \mu \end{array} \right\rangle^* \langle ({t^3_{2g}}^4 A_{2g}; e_g^1) {}^5E_g \| \hat{d} \| (({t^4_{2g}}^3 T_{1g}; e_g^1) {}^4\Gamma_g; \underline{\gamma_u}) {}^5T_u \rangle, \end{aligned} \quad (4)$$

where for the many-electron submatrix element

$$\begin{aligned} & \langle ({t^3_{2g}}^4 A_{2g}; e_g^1) {}^5E_g \| \hat{d} \| (({t^4_{2g}}^3 T_{1g}; e_g^1) {}^4\Gamma_g; \underline{\gamma_u}) {}^5T_u \rangle = \\ & (-1)^{j(\gamma_u)} 3\sqrt{2} [\Gamma_g] \left\{ \begin{array}{ccc} T_2 & A_2 & T_1 \\ E & \Gamma & E \end{array} \right\} \left\{ \begin{array}{ccc} \gamma & T_1 & T_2 \\ E & \Gamma & T \end{array} \right\} \langle \gamma_u \| d \| t_{2g} \rangle : \end{aligned} \quad (5)$$

$\gamma_u \rightarrow e_g$ transfer

$$\begin{aligned} & \langle ({t^3_{2g}}^4 A_{2g}; e_g^1) {}^5E_g \mu | \hat{d}_q | (({t^3_{2g}}^4 A_{2g}; e_g^2, {}^{2S_1+1}\Gamma_{1g}) {}^{2S+1}\Gamma_g; \underline{\gamma_u}) {}^5T_u \mu' \rangle = \\ & (-1)^\mu \left\langle \begin{array}{ccc} E_g & T_{1u} & T_u \\ -\mu & q & \mu \end{array} \right\rangle^* \langle ({t^3_{2g}}^4 A_{2g}; e_g^1) {}^5E_g \| \hat{d} \| (({t^3_{2g}}^4 A_{2g}; e_g^2, {}^{2S_1+1}\Gamma_{1g}) {}^{2S+1}\Gamma_g; \underline{\gamma_u}) {}^5T_u \rangle, \end{aligned} \quad (6)$$

where for the many-electron submatrix element

$$\begin{aligned} & \langle ({t^3_{2g}}^4 A_{2g}; e_g^1) {}^5E_g \| \hat{d} \| (({t^3_{2g}}^4 A_{2g}; e_g^2, {}^{2S_1+1}\Gamma_{1g}) {}^{2S+1}\Gamma_g; \underline{\gamma_u}) {}^5T_u \rangle = \\ & (-1)^{1+j(\gamma_u)+j(\Gamma)} \sqrt{6} [S_1, S, \Gamma_{1g}, \Gamma_g]^{1/2} \left\{ \begin{array}{ccc} 3/2 & S_1 & S \\ 1/2 & 2 & 1/2 \end{array} \right\} \left\{ \begin{array}{ccc} A_2 & E & E \\ E & \Gamma & \Gamma_1 \end{array} \right\} \left\{ \begin{array}{ccc} \gamma & T_1 & E \\ E & \Gamma & T \end{array} \right\} \langle \gamma_u \| d \| e_g \rangle. \end{aligned} \quad (7)$$

Here, the expressions (4),(6) represent the Wigner-Eckart theorem for many-electron transition matrix elements with $\left\langle \begin{array}{ccc} \cdot & \cdot & \cdot \\ \cdot & \cdot & \cdot \end{array} \right\rangle$ being the Wigner coefficient for the cubic point group [16, 19]. In (5),(7) the conventional notations are used for spin $6j$ - and orbital 6Γ symbols ($\left\{ \begin{array}{ccc} \cdot & \cdot & \cdot \\ \cdot & \cdot & \cdot \end{array} \right\}$); $[S] = 2S + 1$, $[\Gamma]$ is the dimensionality of

the corresponding irreducible representation of the cubic point group; $j(\Gamma)$ the so-called quasimomentum number; $\langle \gamma_u \| d \| \gamma_g \rangle$ is the one-electron dipole moment submatrix element. The latter is defined by the respective Wigner-Eckart theorem as follows

$$\langle \gamma_u \mu | \hat{d}_q | \gamma_g \mu' \rangle = (-1)^{j(\gamma_u) - \mu} \begin{Bmatrix} \gamma_u & T_{1u} & \gamma_g \\ -\mu & q & \mu \end{Bmatrix}^* \langle \gamma_u \| d \| \gamma_g \rangle, \quad (8)$$

and could be rather simply evaluated in frames of the so-called "local" approximation, when on calculating the matrix of the dipole moment one neglect all many-center integrals:

$$\langle \phi_{k_1}(\mathbf{R}_1 - \mathbf{r}) | \mathbf{d} | \phi_{k_2}(\mathbf{R}_2 - \mathbf{r}) \rangle = e \mathbf{R}_1 \delta_{\mathbf{R}_1, \mathbf{R}_2} \delta_{\mathbf{k}_1, \mathbf{k}_2},$$

where $\mathbf{R}_1, \mathbf{R}_2$ label sites, $\mathbf{k}_1, \mathbf{k}_2$ atomic functions, respectively. Then

$$\begin{aligned} \langle t_{2u}(\pi) \| d \| e_g \rangle &= 0; \langle t_{2u}(\pi) \| d \| t_{2g} \rangle = -i \sqrt{\frac{3}{2}} \lambda_\pi d; \\ \langle t_{1u}(\sigma) \| d \| t_{2g} \rangle &= 0; \langle t_{1u}(\sigma) \| d \| e_g \rangle = -\frac{2}{\sqrt{3}} \lambda_\sigma d \\ \langle t_{1u}(\pi) \| d \| e_g \rangle &= 0; \langle t_{1u}(\pi) \| d \| t_{2g} \rangle = \sqrt{\frac{3}{2}} \lambda_\pi d. \end{aligned} \quad (9)$$

Here, $\lambda_\sigma, \lambda_\pi$ are covalency parameters for e_g, t_{2g} electrons, respectively, $d = eR_0$ is elementary dipole moment for the cation-anion bond length R_0 . We see, that the "local" approximation results in an additional selection rule: it forbids the $\sigma \rightarrow \pi$, and $\pi \rightarrow \sigma$ transitions, $t_{1u}(\sigma) \rightarrow t_{2g}$, and $t_{1,2u}(\pi) \rightarrow e_g$, respectively, though these are dipole-allowed. In other words, in frames of this approximation only σ -type ($t_{1u}(\sigma) \rightarrow e_g$) or π -type ($t_{1,2u}(\pi) \rightarrow t_{2g}$) CT transitions are allowed. It should be emphasized that the "local" approximation, if non-zero, provides the leading contribution to transition matrix elements with corrections being of the first order in the cation-anion overlap integral. Interestingly, that the one-electron dipole moment submatrix elements for both $\pi \rightarrow \pi$ transitions have the same absolute value. Hereafter, we make use the terminology of "strong" and "weak" transitions for the dipole-allowed CT transitions going on the $\sigma - \sigma$, $\pi - \pi$, and $\pi - \sigma$, $\sigma - \pi$ channels, respectively. Thus, for MnO_6^{9-} center we predict a series of 32 strong many-electron dipole-allowed CT transitions $^5E_g \rightarrow ^5T_{1,2u}$ (24 for $\pi - \pi$, and 8 for $\sigma - \sigma$ channel) and 28 weak dipole-allowed CT transitions ($\pi - \sigma$ and $\sigma - \pi$ cross-channels).

The formulas (5)-(9) together with numerical values for some $6j$ - and 6Γ -symbols, listed below in Appendix allow to make quantitative predictions for relative magnitude of the intensities for different CT transitions. First of all we would like to compare the overall integral intensities for the $\pi - \pi$ and $\sigma - \sigma$ channels of CT transitions. To this end, we calculate and sum the line strengths (the dipole submatrix element squared) which are proportional to the appropriate oscillator strengths:

$$I_{\pi\pi} = 9\lambda_\pi^2 d^2; \quad I_{\sigma\sigma} = \frac{3}{2}\lambda_\sigma^2 d^2, \quad (10)$$

or

$$I_{\pi\pi}/I_{\sigma\sigma} = 6\lambda_\pi^2/\lambda_\sigma^2. \quad (11)$$

In other words, the ratio of the total oscillator strengths for these channels is determined by the ratio of the respective cation-anion charge density transfer parameters. Usually, $\lambda_\sigma^2 > \lambda_\pi^2$, however, it seems the overall intensity for the $\pi - \pi$ channel can exceed that of for $\sigma - \sigma$ channel. In frames of the separate channel we can obtain exact relations between the partial oscillator strengths for the CT transitions differing by the final state of the $t_{2g}^4 e_g^1$ and $t_{2g}^3 e_g^2$ configuration for the $\pi - \pi$ and $\sigma - \sigma$ channel, respectively. For the $\pi - \pi$ channel we have

$$I(^4T_{1g}; ^5T_u) : I(^4T_{2g}; ^5T_u) = \frac{1}{2} : \frac{1}{2} \quad (12)$$

irrespective of the type of the transferred oxygen π electron, t_{2u} , or t_{1u} . Here, each intensity represents the sum for two doublets, $^5T_{1u}$ and $^5T_{2u}$. Interestingly, the relative intensity for these two components is 3 : 1 and 1 : 3 for the $^4T_{1g}$ and $^4T_{2g}$ "intermediate" terms, respectively.

For the $\sigma - \sigma$ channel we have the more nontrivial relation:

$$I(^6A_{1g}; ^5T_u) : I(^4A_{1g}; ^5T_u) : I(^4A_{2g}; ^5T_u) : I(^4E_g; ^5T_u) = \frac{8}{15} : \frac{2}{15} : \frac{2}{9} : \frac{1}{9}, \quad (13)$$

where the last transition is doublet with the equal intensity of both components. It should be reminded that all these numerical data are obtained in frames of the "local" approximation for CT transitions to "pure" $t_{2g}^4 e_g^1$ and $t_{2g}^3 e_g^2$ configurations.

4 Charge transfer transitions in $LaMnO_3$

Now we can apply the model theory to the undoped manganite $LaMnO_3$. For our analysis to be more quantitative we make two rather obvious model approximations. First of all, one assumes that in $LaMnO_3$ as usually for cation-anion octahedra in $3d$ -oxides [9, 10, 11] the non-bonding $t_{1g}(\pi)$ oxygen orbital has the highest energy and forms the first electron removal oxygen state. Moreover, to be definite we assume that the energy spectrum of the nonbonding oxygen states for $Mn^{3+}O_6^{9-}$ centers in $LaMnO_3$ coincides with that calculated in Ref.[11] for $Fe^{3+}O_6^{9-}$ in $LaFeO_3$ with the same crystalline environment, in other words, we have (in eV):

$$\Delta(t_{1g}(\pi) - t_{2u}(\pi)) \approx 0.8; \Delta(t_{1g}(\pi) - t_{1u}(\pi)) \approx 1.8; \Delta(t_{1g}(\pi) - t_{1u}(\sigma)) \approx 3.0.$$

It is believed to be a rather reasonable choice of the energy parameters because the purely oxygen states mainly depend only on crystalline environment. Secondly, we choose for the Racah parameters B and C the numerical values typical for Mn^{2+} in oxides, 0.12 and 0.41 eV, respectively (see above). The crystal-field parameter Dq may be varied, however, we decide in favor of only two model considerations with the same absolute value but the different sign of $|Dq| = 0.15$ eV ("conventional" $Dq > 0$ and "unconventional" $Dq < 0$ sign). Let mention that this value, irrespective the sign, provides a reasonable explanation of the Mn^{2+} spectra in MnO [13] (see above).

Hereafter, this set of parameters is used for the model theoretical simulation of the overall CT band in $LaMnO_3$. Firstly, we argue that the lowest in energy spectral feature observed in $LaMnO_3$ near 1.7 eV is believed to be associated with the onset of the series of the dipole-forbidden CT transitions $t_{1g}(\pi) \rightarrow e_g, t_{2g}$, rather than with any $d - d$ crystal field transition. The energy of this transition was picked out to be a starting point to assign all other CT transitions.

Weakly dipole-allowed $\pi - \sigma$ CT transitions $t_{2u}(\pi) - e_g$ and $t_{1u}(\pi) - e_g$ form more intensive CT bands starting at higher than the preceding series energies, near 2.5 and 3.5 eV, respectively, in accordance with the magnitude of the $t_{1g}(\pi) - t_{2u}(\pi)$ and $t_{1g}(\pi) - t_{1u}(\pi)$ separations. Actually, the $t_{1g}(\pi) - t_{1u}(\pi)$ transition has to be more intensive because the $t_{1u}(\pi)$ state is partly hybridized with $t_{1u}(\sigma)$, hence this transition borrows a portion of intensity from the strong dipole-allowed $t_{1u}(\sigma) - e_g$ CT transition.

The latter $\sigma - \sigma$ transition as we see from Exp.(13) forms intensive broad CT band starting from the main $^5E_g - ^6A_{1g}; ^5T_{1u}$ peak at ≈ 4.7 eV and ranging to the $^5E_g - ^4A_{2g}; ^5T_{1u}$ peak at ≈ 10.2 eV with interstitial peaks at ≈ 8.0 eV being the result of the superposition of two transitions $^5E_g - ^4A_{1g}; ^5T_{1u}$ and $^5E_g - ^4E_g; ^5T_{1u}$, and at ≈ 8.8 eV due to another $^5E_g - ^4E_g; ^5T_{1u}$ transition, respectively. Thus, overall width of the CT bands with final $t_{2g}^3 e_g^2$ configuration occupies a spectral range from 1.7 up to ~ 10 eV.

As it is seen from (12) strong dipole-allowed $\pi - \pi$ CT transitions $t_{2u}(\pi), t_{1u}(\pi) - t_{2g}$ form two manifolds of equally intensive CT bands shifted with respect each other by the $t_{2u}(\pi) - t_{1u}(\pi)$ separation (≈ 1.0 eV). In turn, each manifold consists of two triplets of weakly splitted equally intensive CT bands associated with $^5E_g - ^4T_{1g}; ^5T_u$ and $^5E_g - ^4T_{2g}; ^5T_u$ transitions, respectively. In accordance with the assignment of crystal-field transitions [13] in $LaMnO_3$ (see Fig.2) we should expect the low-energy edge of the dipole-allowed $\pi - \pi$ CT band starting from ≈ 4.5 eV ($1.7 + 2.0 + (t_{1g}(\pi) - t_{2u}(\pi)$ separation)). Taking account of strong configuration interaction we should expect the high-energy edge of this band associated with the highest in energy $^4T_{2g}$ term of the $3d^5$ configuration to be situated near ≈ 9.9 eV. In between, in accordance with our scheme of energy levels we predict peaks at 5.2; 5.5; 6.2 ($\times 2$); 7.2($\times 2$); 7.9; 8.2; 8.3; 8.9 eV. The weakly dipole-allowed $\sigma - \pi$ transitions occupy the high-energy spectral range from 6.7 to 11.1 eV.

Overall, our analysis shows the multi-band structure of the CT optical response in $LaMnO_3$ with the weak low-energy edge at 1.7 eV, associated with forbidden $t_{1g}(\pi) - e_g$ transition and a series of strong bands in the range $4.6 \div 10.2$ eV beginning from composite peak at $\sim 4.5 \div 4.7$ eV and closing by composite peak at $8 \div 10$ eV both resulting from the superposition of strong dipole-allowed $\pi - \pi$ and $\sigma - \sigma$ CT transitions.

As it was mentioned above, the energy spectrum of CT states in MnO_6^{9-} octahedra does not depend on the sign of the crystal-field parameter Dq . However, the intensities of the CT transitions appear to be extremely sensitive to the sign of Dq , or in other words, to the relative energy position of e_g and t_{2g} orbitals. In frames of our model we have performed the theoretical simulation of the overall O2p-Mn3d CT band in MnO_6^{9-} octahedra generated by dipole-allowed CT transitions. For simplicity, we have assumed: i) the equal integral intensities for the $\sigma - \sigma$ and $\pi - \pi$ channels: $I_{\sigma\sigma} = I_{\pi\pi}$, that corresponds $\lambda_\sigma = 6\lambda_\pi$; and ii) the equal integral intensities $I_{\pi\sigma} = I_{\sigma\pi} = 0.1I_{\sigma\sigma}$ for all weakly dipole-allowed transitions $t_{2u}(\pi) - e_g$, $t_{1u}(\pi) - e_g$, and $t_{1u}(\sigma) - t_{2g}$. The results of model calculations are presented in Fig.3a,b for conventional $Dq > 0$ (3a) and unconventional $Dq < 0$ (3b) sign for crystal-field parameter. The top panels in both cases show the partial contributions of different dipole-allowed transitions modeled by rather narrow Lorentzians with $\Gamma = 0.5$ eV to clearly reveal the multiplet structure. The lower panels present the overall contribution to the imaginary part of dielectric function of the dipole-allowed CT transitions. Here, the Lorentzian

linewidth is assumed to be $\Gamma = 1.0$ eV for all contributions to maximally reproduce the experimental situation. All the spectra are presented in the same relative units.

First, one should note that the $\sigma - \sigma$ and $\pi - \sigma$ channels which define the low-energy part of the overall CT band show no change with the Dq sign inversion. However, the $\pi - \pi$ and $\sigma - \pi$ channels manifest anomalously strong dependence on the Dq sign with clearly seen spectral weight transfer from the composite band centered around ~ 5 eV given $Dq > 0$ (Fig.3a) to the composite band centered around ~ 9 eV given $Dq < 0$ (Fig.3b). Thus, the high-energy part of the overall CT band provides a very sensitive tool to examine the screening effects for crystal field in the $3d^5$ configuration with the oxygen hole surrounding.

The theoretical findings are in quantitative agreement with experimental spectra available [3]. Indeed, a rather broad spectral structure with distinctly revealed peaks near 5 eV and $8 \div 9$ eV are observed in the ϵ_2 spectra for undoped $LaMnO_3$ [3] (see insets, Fig.3), although only the band peaked near 5 eV was assigned earlier to the $O2p - Mn3d$ charge transfer. The high-energy peak at $8 \div 9$ eV was assigned by Okimoto *et al.* to $O2p - La5d$ interband transitions [3] albeit this was argued rather on the quantitative considerations than either calculations. However, Arima and Tokura in their optical study of different perovskite-type RMO_3 (R =La, Y, M = Sc, Ti, V, Cr, Mn, Fe, Co, Ni, Cu) [2] have shown that similar band is commonly observed for all both $LaMO_3$ and YMO_3 compounds. In other words, it seems more natural to ascribe this band rather to the high-energy edge of the $O2p$ - $M3d$ CT transitions, than the $O2p$ - $La5d$, $O2p$ - $Y4d$ [2]. Comparing simulated and experimental spectra we may unambiguously assign the high-energy feature around $8 \div 9$ eV to the high-energy edge of the $O2p$ - $Mn3d$ CT transitions. Moreover, comparing the intensities of 5 eV and $8 \div 9$ eV bands, we may state that the oxygen hole in the CT states of MnO_6^{9-} center gives rise to the strong overscreening of the crystal-field parameter Dq resulting in the sign inversion. Nevertheless, we should emphasize that irrespective the numerical value and sign of Dq the low-energy spectral range of the overall CT band consists of a series of transitions with increasing intensity beginning from the lowest dipole-forbidden $t_{1g}(\pi) - e_g$ peaked at 1.7 eV, weakly dipole-allowed $t_{2u}(\pi) - e_g$ peaked at 2.5 eV, relatively more intensive, but weak dipole-allowed $t_{1u}(\pi) - e_g$ peaked at 3.5 eV, and, finally, strong dipole-allowed $t_{1u}(\sigma) - e_g$ transition peaked at 4.7 eV, respectively.

Interestingly, that with slight substitution in doped systems like $La_{1-x}Sr_xMnO_3$ the weak low-energy edge band at 1.7 eV gradually disappears [4, 5] with simultaneous shift of the high-energy bands to the lower frequencies. Our model allows to associate this effect with localization of the doped holes in the upper purely oxygen orbitals like $t_{1g}(\pi)$, $t_{2u}(\pi)$ [1]. Then the lowering of the electron density for these states would result in the lowering of the intensity for the appropriate CT bands. The red shift of the high-energy bands can result from the screening effects induced by oxygen holes mainly for the Racah parameter A .

5 Conclusions

In frames of a rather conventional quantum-chemical approach, which combines the crystal field and the ligand field models we have addressed different CT states and $O2p - Mn3d$ CT transitions in MnO_6^{9-} octahedra. The many-electron dipole transition matrix elements were calculated using the Racah algebra for the cubic point group. Simple "local" approximation allowed to calculate the relative intensity for all dipole-allowed $\pi - \pi$ and $\sigma - \sigma$ CT transitions. We present a self-consistent description of the CT bands in $LaMnO_3$. Our analysis shows the multi-band structure of the CT optical response with the weak low-energy edge at 1.7 eV, associated with forbidden $t_{1g}(\pi) - e_g$ transition and a series of the high-energy weak and strong dipole-allowed high-energy transitions starting from 2.5 and 4.5 eV, respectively, and extending up to nearly 11 eV. The most intensive features are associated with two strong composite bands near $4.6 \div 4.7$ eV and $8 \div 9$ eV, respectively, resulting from the superposition of the dipole-allowed $\sigma - \sigma$ and $\pi - \pi$ CT transitions. These theoretical findings are in quantitative agreement with experimental spectra available. We examined the effects of the sign of the crystal-field parameter Dq and showed that the $\pi - \pi$ and $\sigma - \pi$ channels contrary to $\sigma - \sigma$ and $\pi - \sigma$ ones manifest anomalously strong dependence on the Dq sign with clearly seen spectral weight transfer from the composite band centered around ~ 5 eV given $Dq > 0$ to the composite band centered around ~ 9 eV given $Dq < 0$. Thus, the high-energy part of the overall CT band provides a very sensitive tool to examine the screening effects for crystal-field in the $3d^5$ configuration with the oxygen hole surrounding. The experimental data point to a strong overscreening of the crystal-field parameter Dq in the CT states of MnO_6^{9-} centers. In addition, we would like emphasize the specific role of the intra-atomic correlation effects. It seems, the actual spectral picture of the CT optical response is determined on equal footings both by the intra-atomic $d - d$ electron-electron repulsion and single electron effects. We did not address the inter-center CT transitions. Its role in optical response remains so far unclear, however, appropriate intensities seem to be small because these are proportional to small inter-center $d - d$ transfer integrals squared.

6 Acknowledgments

The discussions with N.N. Loshkareva, Yu.P. Sukhorukov, E.A. Ganshina, V.S. Vikhnin, R. Hayn, S.-L. Drechsler are acknowledged. The research described in this publication was supported in part by grant SMWK of the Ministry of Science and Art of Saxony. The author would like to thank for hospitality Institut für Festkörper- und Werkstoffsorschung Dresden, where part of this work was made. The author acknowledges a partial support from the Award No.REC-005 of the U.S. Civilian Research & Development Foundation for the Independent States of the Former Soviet Union (CRDF), Russian Ministry of Education, grant E00-3.4-280, and Russian Foundation for Basic Researches, grant 01-02-96404.

Appendix: Numerical values for some $6j$ - and 6Γ -coefficients

$$\begin{aligned}
\left\{ \begin{array}{ccc} 3/2 & 1 & 5/2 \\ 1/2 & 2 & 1/2 \end{array} \right\} &= -\frac{1}{\sqrt{15}}; \quad \left\{ \begin{array}{ccc} 3/2 & 1 & 3/2 \\ 1/2 & 2 & 1/2 \end{array} \right\} = \frac{1}{2\sqrt{10}}; \quad \left\{ \begin{array}{ccc} 3/2 & 0 & 3/2 \\ 1/2 & 2 & 1/2 \end{array} \right\} = \frac{1}{2\sqrt{2}}; \\
\left\{ \begin{array}{ccc} A_2 & E & E \\ E & A_1 & A_2 \end{array} \right\} &= \left\{ \begin{array}{ccc} A_2 & E & E \\ E & A_2 & A_1 \end{array} \right\} = -\frac{1}{\sqrt{2}}; \quad \left\{ \begin{array}{ccc} A_2 & E & E \\ E & E & E \end{array} \right\} = \frac{1}{2}; \\
-\left\{ \begin{array}{ccc} T_1 & T_1 & E \\ E & A_1 & T_1 \end{array} \right\} &= \left\{ \begin{array}{ccc} T_1 & T_1 & E \\ E & A_2 & T_2 \end{array} \right\} = \left\{ \begin{array}{ccc} T_2 & A_2 & T_1 \\ E & T_1 & E \end{array} \right\} = \left\{ \begin{array}{ccc} T_2 & A_2 & T_1 \\ E & T_2 & E \end{array} \right\} = -\frac{1}{\sqrt{6}}; \\
\left\{ \begin{array}{ccc} T_2 & T_1 & T_2 \\ E & T_1 & T_2 \end{array} \right\} &= \left\{ \begin{array}{ccc} T_1 & T_1 & T_2 \\ E & T_2 & T_1 \end{array} \right\} = -\left\{ \begin{array}{ccc} T_2 & T_1 & T_2 \\ E & T_2 & T_1 \end{array} \right\} = -\left\{ \begin{array}{ccc} T_1 & T_1 & T_2 \\ E & T_1 & T_2 \end{array} \right\} = \frac{1}{6}; \\
\left\{ \begin{array}{ccc} T_1 & T_1 & E \\ E & E & T_1 \end{array} \right\} &= \left\{ \begin{array}{ccc} T_1 & T_1 & E \\ E & E & T_2 \end{array} \right\} = \left\{ \begin{array}{ccc} T_1 & T_1 & T_2 \\ E & T_2 & T_2 \end{array} \right\} = \\
-\left\{ \begin{array}{ccc} T_1 & T_1 & T_2 \\ E & T_1 & T_1 \end{array} \right\} &= -\left\{ \begin{array}{ccc} T_2 & T_1 & T_2 \\ E & T_1 & T_1 \end{array} \right\} = -\left\{ \begin{array}{ccc} T_2 & T_1 & T_2 \\ E & T_2 & T_2 \end{array} \right\} = \frac{1}{2\sqrt{3}}.
\end{aligned}$$

References

- [1] A.S. Moskvin, I.L. Avvakumov, cond-mat/0108355 (submitted to Physica B).
- [2] T. Arima, Y. Tokura, J. Phys. Soc. Jap. **64**, 2488 (1995).
- [3] Y. Okimoto, T. Katsufui, T. Ishikawa, A. Urushibara, T. Arima, and Y. Tokura, Phys. Rev. Lett. **75**, 109 (1995); Y. Okimoto, T. Katsufui, T. Ishikawa, T. Arima, and Y. Tokura, Phys. Rev. B **55**, 4206 (1997).
- [4] J.H. Jung, K.H. Kim, T.W. Noh et al., Phys. Rev. B **57**, R11043 (1998).
- [5] Koshi Takenaka, Kenji Iida, Yuko Sawaki et al., J. Phys. Soc. Jap. **68**, 1828 (1999).
- [6] J.F. Lawler, J.G. Lunney, and J.M.D. Coey. J. Appl. Phys. Lett. **65**, 3017 (1994).
- [7] I. B. Bersuker, Electronic structure and properties of transition metal compounds (introduction to the theory), New York., Wiley, 1996.
- [8] B.E. Douglas, C.A. Hollingsworth, Symmetry in Bonding and Spectra, Orlando, Acad. Press, 1985.
- [9] C.N.R. Rao, B. Raveau, Transition Metal Oxides, VCH, 1995.
- [10] F.J. Kahn, P.S. Pershan, J.P. Remeika, Phys. Rev. **186**, 891 (1969).
- [11] A.I. Liechtenstein, A.S. Moskvin, V.A. Gubanov, Fizika Tverdogo Tela **24**, 3596 (1982) (in Russian).
- [12] Gen Matsumoto, J. Phys. Soc. Jap. **29**, 615 (1970).
- [13] B. Fromme, U. Brunokowski, and E. Kisker, Phys. Rev. B **58**, 9783 (1998).
- [14] L.E. Orgel, J. Chem. Phys. **23**, 1004 (1955); G.W. Pratt, Phys. Rev. **116**, 281 (1959).
- [15] J. van Elp, R.H. Potze, H. Eskes, R. Berger, and G.A. Sawatzky, Phys. Rev. B **44**, 1530 (1991).

- [16] Y. Tanabe, S. Sugano, H. Kamimura, Multiplets of Transition Metals in Crystals. N.Y.:Acad. Press., 1971; T. Inui, Y. Tanabe, Y. Onodera, Group Theory and its Application in Physics, Springer-Verlag, Berlin-Heidelberg, 1990.
- [17] A.S. Davydov, Theory of Molecular Excitons, McGraw-Hill, New York, 1962.
- [18] D. A. Varshalovich, A. N. Moskalev, V. K. Khersonskii. Quantum Theory of Angular Momentum (World Scientific, Singapore, 1988).
- [19] We make use of the Racah algebra for cubic point group in the form developed by Lituanian school (see e.g. I.V. Batarunas, I.B. Levinson, Tr. AN Lit.SSR, ser. B, 2(22), Vilnius, 1960, s.15). For a rather complete summary of this approach, see e.g. A.S. Moskvin, I.G. Bostrem, Metod Neprivodimykh Tenzornykh Operatorov Tochechnykh Grup (Method of Irreducible Tensorial Operators for Point Groups), Uralskiy Universitet, Ekaterinburg, 1998, 106 s.

Figure captions

Fig.1. The diagram of Mn3d-O2p molecular orbitals for the MnO_6 octahedral center. By arrows the Mn3d-O2p charge transfer transitions are shown: thick solid arrows – strongly dipole-allowed $\sigma - \sigma$ and $\pi - \pi$; thin solid arrows – weakly dipole-allowed $\pi - \sigma$ and $\sigma - \pi$; thin dashed arrows – weak dipole-forbidden low-energy transitions, respectively.

Fig.2. The energy-level Tanabe-Sugano diagram for the high-spin terms of $3d^5$ configuration in octahedral (or cubic) crystal field.

Fig.3. Theoretical simulation of the overall O2p-Mn3d CT band in $LaMnO_3$ with conventional $Dq > 0$ (3a) and unconventional $Dq < 0$ (3b) sign for crystal-field parameter. The top panel shows partial contributions of different dipole-allowed transitions modeled by rather narrow Lorentzians with $\Gamma = 0.5$ eV to clearly reveal the multiplet structure. The lower panel presents the overall contribution to the imaginary part of dielectric function of the dipole-allowed CT transitions. Here, the Lorentzian linewidth is assumed to be $\Gamma = 1.0$ eV for all contributions to maximally reproduce the experimental situation. All the spectra are presented in the same relative units. Arrow marks the position of the lowest in energy dipole-forbidden transition $t_{1g}(\pi) - 3d$. Experimental spectrum for $La_{1-x}Sr_xMnO_3$ given $x \approx 0$ [3] is shown in inset. See text for details.

